Phase diagram of self-attracting systems

P.H. Chavanis[1] and I. Ispolatov[2]
[1] *Laboratoire de Physique Quantique, Université Paul Sabatier, 118 route de Narbonne 31062 Toulouse, France*
[2] *Departamento de Fisica, Universidad de Santiago de Chile, Casilla 302, Correo 2, Santiago, Chile*

Phase diagram of microcanonical ensembles of self-attracting particles is studied for two types of short-range potential regularizations: self-gravitating fermions and classical particles interacting via attractive soft $-(r^2+r_0^2)^{-1/2}$ Coulomb potential. When the range of regularization is sufficiently short, the self-attracting systems exhibit gravitational or collapse-like transition. As the fermionic degeneracy or the softness radius increases, the gravitational phase transition crosses over to a normal first-order phase transition, becomes second-order at a critical point, and finally disappears. Applicability of a commonly used saddle-point or mean-field approximation and importance of metastable states is discussed.

PACS numbers: 64.60.-i 02.30.Rz 04.40.-b 05.70.Fh

I. INTRODUCTION

Ensembles of particles interacting via a long-range non-integrable attractive potential, $U(r) = Ar^{-\alpha}$, $A < 0$, and $0 < \alpha < 3$, are known to exhibit gravitational phase transition between a relatively uniform high energy state and a low-energy state with a core-halo structure [1, 2, 3, 4, 5, 6, 7, 8, 9, 10, 11, 12]. It has also been established [4, 5, 6, 7, 8, 9, 10] that if the interaction potential has some form of short range cutoff, the density and all other physical quantities that characterize the core-halo state are finite, while for a bare $r^{-\alpha}$ attractive potential the collapse results in a singular state with an infinite density, entropy and free energy. The gravitational phase transitions are known to exist in microcanonical, canonical, and grand canonical ensembles; yet the details of the phase transition and the structure of the core-halo state are ensemble-dependent. In this paper we shall essentially consider microcanonical ensembles; for long-range interacting systems they are known to have richer phenomenology and allow for states (such as ones with a negative specific heat) that are inaccessible in both canonical and grand canonical ensembles. In addition, the microcanonical ensemble is the most fundamental since the notion of thermostat is ambiguous for long-range interacting systems.

A typical entropy vs. energy plot, describing a gravitational phase transition in a microcanonical ensemble, is shown in Fig. 1, lower plot [5, 6, 7, 8, 10]. High-energy and low-energy branches correspond to the uniform and to the core-halo states, respectively; their intersection E^* marks the point of the phase transition. Metastable uniform and core-halo states, shown by dashed lines, exist in the energy intervals $[E_1, E^*]$ and $[E^*, E_2]$, correspondingly. When the energy is larger than E_2, the system can be only in the stable uniform state. The system still stays in this uniform state after energy is decreased past E^* and the uniform state becomes metastable. When the energy reaches E_1, the uniform state becomes unstable and the system undergoes a collapse to a stable core-halo state. During such a collapse the entropy is discontinuously increased, and the macroscopic rearrangement of the density profile occurs. Similarly, the core-halo state is stable below E^*, metastable between E^* and E_2, and undergoes a discontinuous transition reverse to the collapse, at E_2. This transition is sometimes called an explosion [5], since it transforms the dense core into a relatively uniform mass distribution.

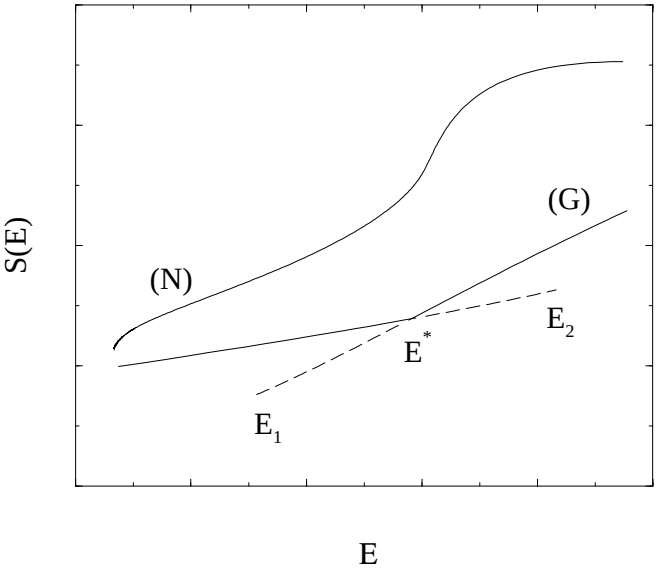

FIG. 1: Sketch of an entropy vs. energy plot for a microcanonical self-attracting system with a short-range cutoff which exhibits a gravitational (G) phase transition. Stable states and metastable states are shown by solid and dashed lines, respectively. Points E_1, E^*, and E_2 denote the collapse energy for the uniform state, the energy of the phase transition, and the energy for which the metastable core-halo state becomes unstable, correspondingly. A typical entropy vs. energy plot for a microcanonical long-range interacting system with a normal (N) first-order phase transition is also shown.

In some sense, the way the gravitational phase transition occurs in a microcanonical ensemble resembles a hysteresis phenomenon that takes place during a first-order phase transition in a canonical ensemble. For this reason,

it is sometimes called a *gravitational* first order phase transition. Yet in a microcanonical ensemble a *normal* first-order phase transition occurs without the hysteresis and metastable states. A distinct feature of a normal microcanonical first-order phase transition in a small or long-range interacting system is a convex dip in otherwise concave continuous entropy plot (see, for example, [13, 14, 15]) sketched in Fig. 1, upper plot (N). Differences between gravitational and normal first-order phase transitions are evident immediately: for a gravitational phase transition the microcanonical inverse temperature $\beta \equiv dS/dE$ is discontinuous at E^* while for the normal first-order phase transition dS/dE is always continuous. In addition, in a gravitational phase transition, the uniform and the core-halo phases cannot coexist, while for the normal first-order phase transition the phases do coexist in a range of energies corresponding to the convex dip.

It has been noticed [5, 6, 7, 8, 10] that the gravitational phase transitions in self-attracting systems exist only when the range of the cutoff is sufficiently small. When the effective cutoff radius is increased, the range of existence of metastable states $[E_1, E_2]$ shrinks and finally disappears along with the dS/dE discontinuity at E^*. The resulting entropy vs. energy plot becomes continuous and qualitatively resembles a corresponding plot for a system with a normal first-order phase transition [8, 10]. This was observed in self-gravitating systems with various short-range regularizations: central excluded volume [7], hard sphere repulsion for individual particles [5], soft-core interaction potential [8], and exclusion due to Fermi-Dirac statistics [6, 10].

In this paper we study how the behavior of self-attracting systems depends on the effective short-range cutoff radius. We find that once the cutoff is increased above a certain value, the gravitational phase transition crosses over to a normal first-order phase transition, characterized by a convex dip in the entropy vs. energy plot and associated with an energy interval with a negative specific heat. As the effective cutoff radius is increased even further, the system reaches a critical point where the first-order phase transition is replaced by a second-order one, and for even larger cutoff radii there is no phase transition at all. To reveal that such a phase diagram is a generic feature of all self-attracting systems, we consider two different examples: an ensemble of self-gravitating particles with Fermi-Dirac exclusion statistics, and a particle system with classical statistics interacting via a soft Coulomb potential $-(r^2 + r_0^2)^{-1/2}$. Since both of these examples have been studied in the past, in the following two sections we present only short outlines of the derivation of the main formulas and refer readers to [6, 8, 9, 10] for a more detailed description. After analyzing these two examples, we discuss the validity of the saddle-point or mean-field approximation, which is commonly used to study self-gravitating systems; a conclusion which summarizes the presented results completes the paper.

II. SELF-GRAVITATING FERMIONS

We consider a microcanonical ensemble of $N \gg 1$ identical unit mass fermions confined to a spherical container of radius R. A simple combinatorial analysis gives for the number of microscopic states W of a Fermi-Dirac system with a phase space distribution function $f(\mathbf{r}, \mathbf{p})$:

$$W[f] \approx \exp\left\{-\frac{g}{(2\pi\hbar)^3}\int [n\ln n + (1-n)\ln(1-n)]d^3\mathbf{r}\,d^3\mathbf{p}\right\}. \quad (1)$$

Here $n(\mathbf{r}, \mathbf{p}) \equiv (2\pi\hbar)^3 f(\mathbf{r}, \mathbf{p})/g$; g is a number of internal degrees of freedom, $g = 2s + 1$ for a particle with spin s. The logarithm of Eq. (1) is the Fermi-Dirac entropy. The most probable distribution expected at equilibrium is obtained by maximizing Eq. (1) with respect to n with the constrained total energy E and number of particles N. The validity of this mean-field approach is discussed in Sec. IV. Expressing the particle density through the Laplacian of the gravitational field by using the Poisson equation, it is found that the mean-field gravitational potential $\phi(\mathbf{r})$ satisfies an equation of the form

$$\Delta\phi(\mathbf{r}) = \frac{4\pi G g}{(2\pi\hbar)^3}\int \frac{d^3\mathbf{p}}{1 + e^{[p^2/2 + \phi(\mathbf{r}) - \nu]/T}}, \quad (2)$$

where G is the gravitational constant. The temperature $T(E, M)$ and the chemical potential $\nu(E, M)$ appear as Lagrange multipliers associated with the conservation of energy and mass. We assume a spherical symmetry of the mean-field potential, introduce a dimensionless radius $\xi \equiv r(Gg\sqrt{8T}/\pi\hbar^3)^{1/2}$, a non-negative dimensionless potential $\psi(\xi) \equiv [\phi(r) - \phi(0)]/T$, and a positive constant $k \equiv \exp\{[\phi(0) - \nu]/T\}$. Then Eq. (2) is reduced to the form [6]:

$$\frac{d^2\psi}{d\xi^2} + \frac{2}{\xi}\frac{d\psi}{d\xi} = I_{1/2}[ke^{\psi(\xi)}]. \quad (3)$$

Here $I_{1/2}$ denotes the Fermi integral

$$I_\sigma(t) = \int_0^{+\infty} \frac{x^\sigma}{1 + te^x}dx. \quad (4)$$

Boundary conditions $\psi(0) = 0$ and $\psi'(0) = 0$ follow from the definition of the potential $\psi(\xi)$ and spherical symmetry, respectively. Using the Gauss theorem for the gravitational potential at the boundary of the spherical container R, the number of particles constraint can be expressed as

$$\frac{d\psi}{dr}(R) = \frac{GM}{TR^2}. \quad (5)$$

Introducing a dimensionless maximum radius $\alpha \equiv R(Gg\sqrt{8T}/\pi\hbar^3)^{1/2}$, we reduce Eq. (5) to the form

$$\alpha^5\psi'(\alpha) = \mu^2, \quad (6)$$

where $\mu \equiv \sqrt{8g^2G^3MR^3/\pi^2\hbar^6}$ is a degeneracy parameter [6], which is proportional to the ratio of the gravitational Fermi energy (defined in Eq. (7) below) to the average gravitational energy GM^2/R to the power 3/2. In the large-μ limit the system becomes completely non-degenerate or classical, and Eq. (2) then reduces to the Boltzmann-Poisson equation. Yet for any finite μ and sufficiently low energy the system is degenerate and mimics the structure of a white dwarf star [16]. In the completely degenerate limit $T \to 0$, the equation for the gravitational potential becomes the Lane-Emden equation for a polytrope of index $n = 3/2$ [16]. The density goes to zero at a finite radius R_* related to the total mass M by the relation $MR_*^3 = 91.869\hbar^6G^{-3}(2/g)^2$. The energy of this fermion ball is given by the Ritter's formula $E = -(3/7)GM^2/R_*$. Hence the minimal possible energy of a self-gravitating degenerate gas, i.e. the gravitational Fermi energy is

$$E_{min} = -5.98\ 10^{-2} g^{2/3} \frac{G^2M^{7/3}}{\hbar^2}. \qquad (7)$$

Note that contrary to the completely degenerate ($E = E_{min}$) case, the density of the self-gravitating Fermi gas for $E > E_{min}$ decreases like r^{-2} at large distances, similarly to the classical self-gravitating isothermal gas. Hence the container is necessary to confine the system [17].

As in [6], we introduce a dimensionless energy ϵ, a dimensionless inverse temperature β, and the entropy per particle s, and express them through α, μ, ψ and k as

$$\begin{aligned} \epsilon \equiv \frac{ER}{GM^2} &= -\frac{\alpha^7}{\mu^4}\int_0^\alpha I_{3/2}[ke^{\psi(\xi)}]\xi^2 d\xi \\ &\quad + \frac{2\alpha^{10}}{3\mu^4} I_{3/2}[ke^{\psi(\xi)}], \\ \beta \equiv \frac{GM}{RT} &= \frac{\mu^2}{\alpha^4}, \\ s \equiv \frac{\ln W}{M} &= \frac{7}{3}\epsilon\beta + \psi(\alpha) + \beta + \ln k \\ &\quad - \frac{2\alpha^6}{9\mu^2} I_{3/2}[ke^{\psi(\alpha)}]. \end{aligned} \qquad (8)$$

Hence, all the thermodynamics parameters ϵ, s, and β are single-valued functions of the degeneracy parameter μ and the uniformization variable k, which continuously parametrizes the functions $\psi(\xi)$. We select a degeneracy μ, and for each k we numerically integrate Eq. (3) for $0 \le \xi \le \alpha$, where α is determined by Eq. (6). Once $\psi(\xi)$ is computed, $\epsilon(k)$, $\beta(k)$, and $s(k)$ are calculated using Eq. (8). The curves giving the entropy $s(k)$ vs. energy $\epsilon(k)$ and the inverse temperature $\beta(k) = ds/d\epsilon$ vs. energy $\epsilon(k)$ are thus defined in a parametric form for various values of the degeneracy parameter μ (see Figs. 2-7).

In the classical $\mu \to +\infty$ limit, the (ϵ, β) plot forms a spiral which winds up indefinitely around a limit point corresponding to the singular isothermal sphere with the energy $\epsilon = -1/4$ and inverse temperature $\beta = 2$ [17]. For very high but finite values of μ, such as $\mu = 10^9$ in Fig. 2, the system is almost non-degenerate and its β vs. ϵ plot looks very similar to this infinite winding spiral. Yet as μ is finite, the spiral is finite as well and does unwind after a turning point. Each point with a vertical tangent (where $d\beta/d\epsilon = \infty$) on the β vs. ϵ spiral corresponds to a cusp in the s vs. ϵ plot. However, all the exotic features

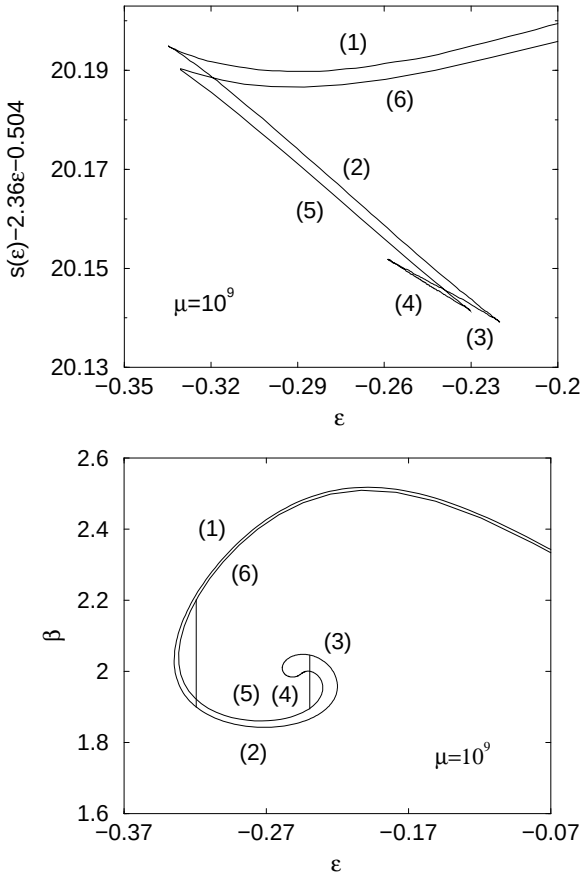

FIG. 2: Plots of entropy per particle $s(\epsilon)$ (upper plot) and dimensionless inverse temperature $\beta(\epsilon) = ds/d\epsilon$ (lower plot) for $\mu = 10^9$. A change of stability of the corresponding state occurs each time the (ϵ, β) spiral has a vertical tangent and the (ϵ, s) plot has a cusp. A mode of stability is lost at the vertical tangent if the curve rotates anticlockwise and gained if the curve rotates clockwise [18]. Therefore, the branches (1) and (7) are stable, (2) and (6) are unstable against one mode, (3) and (5) against two modes and (4) against three modes (branch (7) is not represented in the figure but is the continuation of branch (6) after the turning point of energy at $\epsilon \simeq 147$). There exists values of energy at which the branches with the same degree of instability have the same entropy. It occurs at the crossing points of the s vs ϵ plot and corresponding vertical lines in the β vs ϵ plot. As $\mu \to +\infty$, there are more and more crossing points at energies ϵ_n converging to the value $\epsilon = 1/4$ of the singular isothermal sphere. These points (ϵ_n, s_n) can be associated with points of phase transitions; however, these "phase transitions" occur between unstable states and are therefore unphysical.

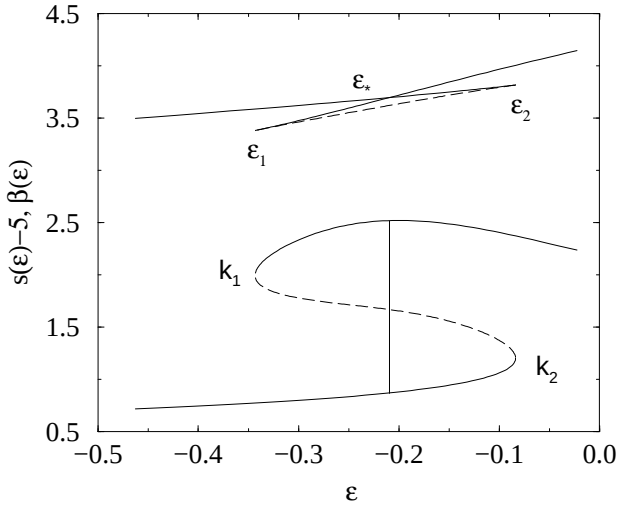

FIG. 3: Plots of entropy per particle $s(\epsilon) - 5$ (top) and dimensionless inverse temperature $\beta(\epsilon) = ds/d\epsilon$ (bottom) for $\mu = 10^4$. Unstable state is shown by dashed lines.

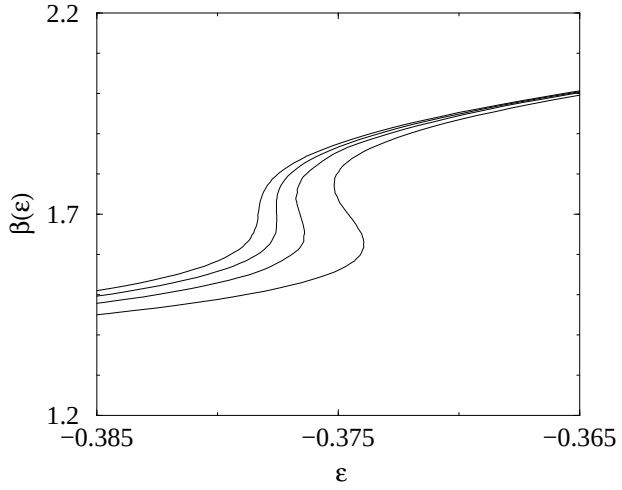

FIG. 4: Plots of inverse temperature $\beta(\epsilon) = ds/d\epsilon$ for (left to right) $\mu = 2.65\times10^3$, 2.67×10^3, 2.7×10^3, and 2.75×10^3. The gravitational phase transition disappears for $\mu < \mu_{gr} = 2.67\times10^3$ and is replaced by a normal first order phase transition.

of the high-μ plots, such as multiply-winding spirals and corresponding multiple kinks are related to unstable and therefore physically unrealizable states [18].

As the degeneracy parameter μ is decreased, the number of unstable states is decreased as well. As illustrated in Fig. 3, for $\mu = 10^4$ there is only one unstable state, shown on the plot by a dashed line. Yet for $\mu = 10^4$ the system is still highly non-degenerate and exhibits all signs of the gravitational phase transition. The low-energy branch of the plot corresponds to the core-halo state which exists for $0 < k < k_2$ and $\epsilon_{min} < \epsilon < \epsilon_2$, where $\epsilon_{min} = -6.42\ 10^{-2}\mu^{2/3}$, is the dimensionless gravitational Fermi energy. Numerical evidence suggests that at the ϵ_2-cusp, both energy $\epsilon(k)$ and entropy $s(k)$ behave as $\mathcal{O}(k-k_2)^2$, which explains the divergence of $d\beta/d\epsilon$, evident in the plot. For $k_2 < k < k_1$ the entropy $s(k)$ is not even a local maximum [6, 10] so the corresponding state, marked by the dashed line in Fig. 3, is unstable. When the curve approaches the second cusp at $\epsilon_1 = \epsilon(k_1)$, both energy ϵ and entropy s go through a $\mathcal{O}[(k-k_1)^2]$ asymptotics again. For $k > k_1$ the equilibrium states, now belonging to the uniform phase, are at least locally stable.

When μ gets smaller and the degeneracy becomes more important, the interval between ϵ_1 and ϵ_2 decreases and finally disappears. In Fig. 4 we plot β vs. ϵ and seek μ such that the $\beta(\epsilon)$ curve loses its characteristic for large μ backbend. This can be viewed as a complete straightening of the classical spiral and happens when $\mu = \mu_{gr} \approx 2.67 \times 10^3$. For $\mu < \mu_{gr}$ the system exhibits a normal first-order phase transition. To illustrate this, in Figs. 5-6 we present entropy and inverse temperature plots for $\mu = 10^3$; signs of microcanonical first-order phase transition such as convex entropy dip and region of negative specific heat where $d^2s/d\epsilon^2 > 0$ are clearly visible.

As we decrease the degeneracy parameter μ even further, the convex dip in the entropy vs. energy plot and correspondingly the interval where $d^2s/d\epsilon^2 > 0$ get narrower, and for $\mu = \mu_{cr} \approx 83$ they disappear (Fig. 7). At $\mu = \mu_{cr}$ the equation $d^2s/d\epsilon^2 = 0$ has only one real root, $\epsilon = \epsilon_{cr} \approx -0.5$, a critical point where the two phases become indistinguishable and the heat capacity diverges. This corresponds to the line of first-order phase transitions in (ϵ, μ) space, terminated by the critical point at $(\epsilon_{cr}, \mu_{cr})$ where the phase transition is second order (see Fig. 11).

For $\mu < \mu_{cr}$, the inverse temperature $\beta(\epsilon)$ is a monotonically decreasing function of energy ϵ and the system does not exhibit any phase transition. Therefore, as the degeneracy parameter decreases, the microcanonical ensemble of self-gravitating fermions consecutively exhibits gravitational, first-order, second-order, and no phase transition at all. Additional discussion of phase transitions in the self-gravitating Fermi gas can be found in Ref. [10].

III. SELF-ATTRACTING PARTICLES WITH SOFT COULOMB POTENTIAL

In this section, we consider phase transitions in another self-attracting system where the short-range cutoff is explicitly present in the interaction potential. As in Sec. II, we consider a microcanonical ensemble of $N \gg 1$ identical unit mass particles confined to a spherical container of radius R, but now the particles obey classical statistics and interact via the attracting soft Coulomb potential $-G/(r^2 + r_0^2)^{-1/2}$. This potential has been used in various numerical simulations of self-gravitating systems and

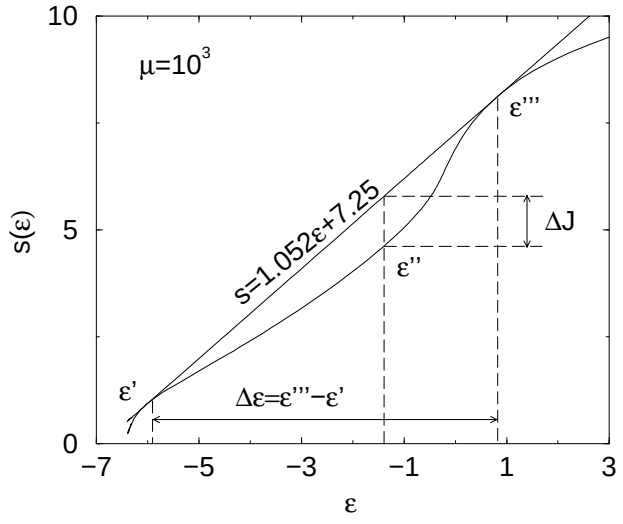

FIG. 5: Plot of entropy s vs. energy ϵ for $\mu = 10^3$. The entropy presents a convex intruder between ϵ' and ϵ'''. For an extensive system, this convex intruder is forbidden because the system with energy $\bar{\epsilon}$, $\epsilon' < \bar{\epsilon} < \epsilon'''$, would gain entropy by splitting in two phases with energy ϵ' and ϵ'''. Indeed, $s(\bar{\epsilon} = \alpha\epsilon' + (1-\alpha)\epsilon''') \leq \alpha s(\epsilon') + (1-\alpha)s(\epsilon''')$, where $0 \leq \alpha \leq 1$ parametrizes the energy $\bar{\epsilon}$ of the systems in the phase coexistence range $[\epsilon', \epsilon''']$. However, for a non-extensive system, such as a gravitational system, this argument does not hold and a convex intruder for the entropy is allowed in the microcanonical ensemble [13].

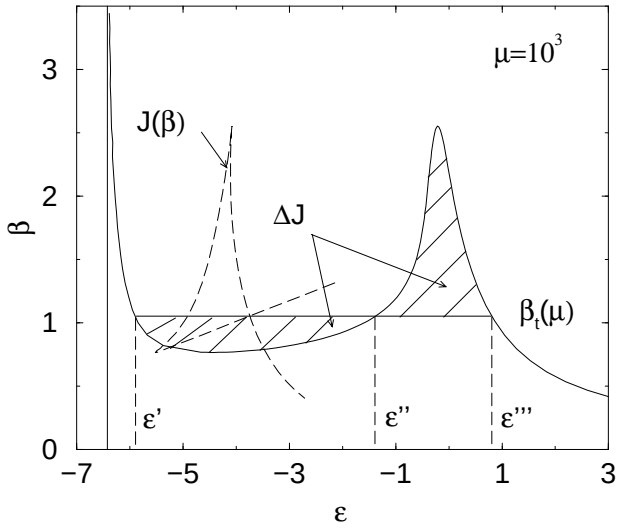

FIG. 6: Plot of inverse temperature $\beta(\epsilon) = ds/d\epsilon$ vs. energy ϵ for $\mu = 10^3$. The existence of negative specific heats $C = -\beta^2 d\epsilon/d\beta < 0$ and the convex intruder for the entropy are the signal of a normal first order phase transition and of the *inequivalence* of statistical ensembles. Indeed, for nonextensive systems, the region of negative specific heat is allowed in the microcanonical ensemble while it is forbidden in the canonical ensemble and replaced by a sharp phase transition (horizontal plateau). The temperature of the transition β_t^{-1} is determined by the crossing point in the free energy $J = s - \beta\epsilon$ vs inverse temperature β plot (dashed line). Alternatively, it can be obtained by performing a Maxwell construction in the β vs ϵ diagram, noting that $\int_{\epsilon_1}^{\epsilon_3}(\beta - \beta_t)d\epsilon = J''' - J' = 0$ (the areas of the shaded regions are $-\Delta J = J'' - J'$ and $\Delta J = J''' - J''$). It is also given by the slope of the straight line $s_{hull}(\epsilon)$ in Fig. 5 ($s_{hull} = a\epsilon + b$ with $a = \beta_t$ and $b = J' = J'''$) [13]. During the canonical phase transition, a latent heat $\Delta\epsilon = \epsilon''' - \epsilon'$ is released.

is also called the Plummer potential. Since such potential does not satisfy the Poisson equation, the equation for the mean-field density or potential cannot be reduced to a differential equation similar to Eq. (2). In this section, we use the integral equation approach suggested in Ref. [8]. The entropy $S(E)$ of the system is defined as the logarithm of the density of states with the energy E,

$$S(E) = \log\left\{\frac{1}{N!}\int\cdots\int\prod_{k=1}^{M}\frac{d^3\mathbf{p}_k\, d^3\mathbf{r}_k}{(2\pi\hbar)^3} \times\delta\left[E - \sum_{l=1}^{M}\frac{p_l^2}{2} + \sum_{i=1}^{M}\sum_{j=1+1}^{M}\frac{G}{\sqrt{(\mathbf{r}_i-\mathbf{r}_j)^2 + r_0^2}}\right]\right\}. \quad (9)$$

Following the steps described in Refs. [8, 9], we integrate Eq. (9) on momenta, express the remaining configurational integral through a functional integral over possible density profiles $\rho(\mathbf{r})$, apply the saddle-point approximation, and introduce the dimensionless coordinate $\mathbf{x} \equiv \mathbf{r}/R$, soft potential radius $x_0 \equiv r_0/R$, and energy per particle $\epsilon \equiv ER/GM^2$. The saddle-point density profile $\rho_s(\mathbf{x})$ satisfies the following integral equation

$$\rho_s(\mathbf{x}) = \rho_0 F[\rho_s(.), \mathbf{x}],$$
$$F[\rho_s(.), \mathbf{x}] = \exp\left[\beta\int\frac{\rho_s(\mathbf{x}')}{\sqrt{(\mathbf{x}-\mathbf{x}')^2 + x_0^2}}d^3\mathbf{x}'\right],$$
$$\beta = \frac{3}{2}\left[\epsilon + \frac{1}{2}\int\int\frac{\rho_s(\mathbf{x}_1)\rho_s(\mathbf{x}_2)}{\sqrt{(\mathbf{x}_1-\mathbf{x}_2)^2 + x_0^2}}d^3\mathbf{x}_1 d^3\mathbf{x}_2\right]^{-1},$$
$$\rho_0 = \left[\int F[\rho_s(.), \mathbf{x}]d^3\mathbf{x}\right]^{-1}. \quad (10)$$

Neglecting an energy-independent constant, the saddle-point entropy per particle $s(\epsilon) \equiv S(\epsilon)/M$ is expressed as

$$s(\epsilon) = -\frac{3}{2}\ln\beta - \int\rho_s(\mathbf{x})\ln[\rho(\mathbf{x})]d^3\mathbf{x}, \quad (11)$$

where β, introduced in Eq. (10), is the inverse dimensionless temperature $\beta(\epsilon) = ds/d\epsilon$. In order to solve Eqs. (10), we assume spherical symmetry of ρ, integrate

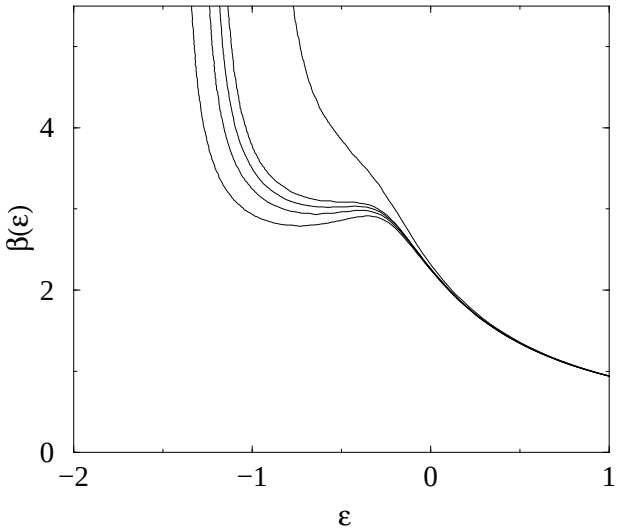

FIG. 7: Plots of inverse temperature $\beta(\epsilon) = ds/d\epsilon$ vs. energy ϵ for (left to right) $\mu = 100$, 90, 85, 80, and 50. The normal first order phase transition disappears for $\mu \leq \mu_{cr} \approx 83$. At the critical value $\mu = \mu_{cr}$ the system passes by a second order phase transition.

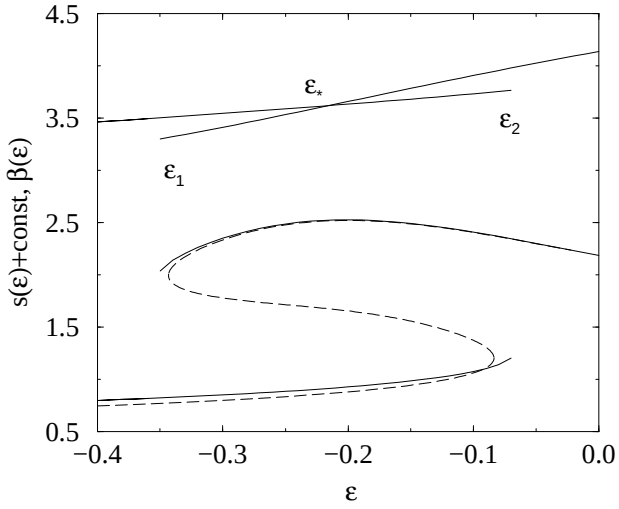

FIG. 8: Plots of entropy $s(\epsilon)$ (top) and inverse temperature $\beta(\epsilon) = ds/d\epsilon$ (bottom) vs. energy ϵ for the soft potential radius $x_0 = 10^{-2}$. Plot of $\beta(\epsilon)$ for the fermionic system with $\mu = 10^4$ is shown in dashed line.

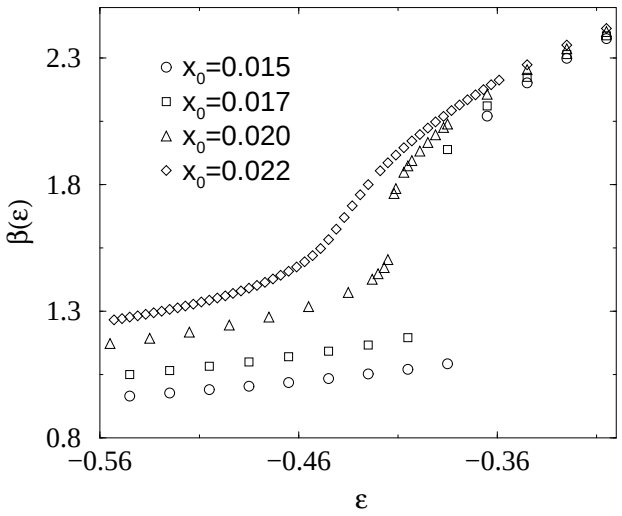

FIG. 9: Plots of inverse temperature $\beta(\epsilon) = ds/d\epsilon$ vs. energy ϵ for different soft potential radii.

Eqs. (10) over angular variables and introduce a map [8]:

$$\rho_{i+1}(x) = \sigma\rho_0 F[\rho_i(.), x] + (1-\sigma)\rho_i(x) \qquad (12)$$

which we iterate numerically. Here $F[\rho(.), x]$ and ρ_0 are defined in Eqs. (10); $0 < \sigma \leq 1$ is a positive step parameter. For convergence, the step parameter is usually set to $\sigma \sim 10^{-1}$. As pointed out in Ref. [8], the integral equation method outlined above allows to obtain density profiles corresponding only to thermodynamically stable or metastable states; for unstable states the iterations defined by Eq. (12) diverge for any σ.

The results in the form of $s(\epsilon)$ vs. ϵ and $ds/d\epsilon$ vs. ϵ plots for various soft potential radii x_0 are presented in Figs 8-10. In Fig. 8 we show the entropy and inverse temperature plots for a relatively small soft potential radius, $x_0 = 10^{-2}$. For this value of x_0 the system clearly exhibits all signs of gravitational phase transition. For comparison, in the same figure we present the $\beta(\epsilon)$ plot for a low-degeneracy fermionic system with $\mu = 10^4$ from Fig. 3. Despite the completely different nature of the short-range cutoffs for these systems, their uniform state entropies exhibit a strikingly similar behavior. This once again illustrates that properties of a uniform state are determined mostly by the long-range properties of the interaction. Naturally, the core-halo state structure and its properties depend on the nature of the cutoff, so the corresponding branches in the entropy vs. energy plot are visually different. Nevertheless, the difference is weak so the physical properties of phase transitions in long-range self-attracting systems are relatively insensitive to the precise form of the small-scale regularization.

Similarly to the fermionic system, as the range of the cutoff is increased, the range of existence of metastable states shrinks and finally disappears. At this point the gravitational phase transition crosses over to the first-order one. From the data presented in Fig. 9 we estimate that this crossover happens at $x_0 = x_{gr} \approx 0.021$. For $x_{gr} < x_0 < x_{cr}$ the system exhibits a normal first-order phase transition until the critical point (ϵ_{cr}, x_{cr}) is reached. The plots presented in Fig. 10 indicate that $\epsilon_{cr} \approx -0.7$ and $x_{cr} \approx 0.22$. When $x_0 > x_{cr}$, no phase transitions are present in the system. This allows us to conclude that similarly to the fermionic system, as the soft potential radius is increased, the self-attracting system with soft Coulomb interaction exhibits consecutively gravitational, first-order, second-order, and no

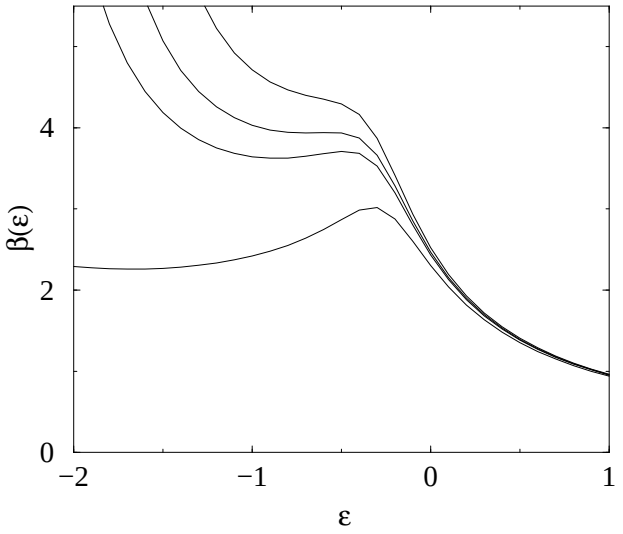

FIG. 10: Plots of inverse temperature $\beta(\epsilon) = ds/d\epsilon$ vs. energy ϵ for the soft potential radii (bottom to top) $x_0 =$ 0.12, 0.2, 0.22, and 0.25.

phase transition at all.

IV. VALIDITY OF MEAN FIELD APPROXIMATION

To obtain the plots shown in Figs. 2-10 we used the saddle point or the mean-field approximation. It raises an important question of whether the distinct features of the gravitational phase transition described above are intrinsic or appear as artifacts of this approximation. Before the approximation is applied, the microcanonical entropy $S(E, N)$ is expressed through the logarithm of a sum of microscopic densities of states W_i of all macroscopic states with the energy E and number of particles N ($k_B = 1$). The mean-field approximation is equivalent to replacing a sum of contributions from these macroscopic states, usually represented by a functional integral over corresponding density (or phase space density) profiles ρ, by a contribution from the single state or density profile ρ_0 [4, 9, 19]:

$$S = \ln \sum_i W_i \sim \ln \int \mathcal{D}\rho \; W[\rho] \approx \ln W[\rho_0]. \qquad (13)$$

This state ρ_0 extremizes the density of states W and, consequently, the entropy S. The condition

$$\left. \frac{\delta W}{\delta \rho} \right|_{\rho=\rho_0} = 0, \qquad (14)$$

defines ρ_0 that gives a global maximum, a local maximum, or a minimum (or saddle point) to the entropy which correspond to stable, metastable, or unstable states, respectively. Let us first consider the range of energies, ($E < E_1$ and $E > E_2$ in Figs. 3 and 8, or all energies in Figs. 7 and 10, for which there exists only one global entropy maximum. This case is described in traditional textbooks of thermodynamics: the single equilibrium state corresponds to a very sharp maximum in the density of states and the first-order corrections to the entropy per particle s scales as $1/N$, i.e. $s = s[\rho_0] + \mathcal{O}(1/N)$. When stable and metastable states coexist ($E_1 < E < E_2$), the mean-field approximation is also an asymptotically exact approximation for the stable states, since the relative contributions from the metastable states ρ_m to $W[\rho]$ scales as $\exp\{N(s[\rho_m] - s[\rho_0])\}$ However, the sharp kink in the mean-field entropy plot at E^* (as in Fig. 1) appears in the true, non-mean-field entropy plot only in the $N \to \infty$ limit; as for any finite number of particles the metastable states contribute significantly to $W[\rho]$ in the vicinity of E^*, where $s[\rho_m] - s[\rho_0] \to 0$. Similarly, the mean-field approximation works well for the metastable states when they are sharp local maxima of $W[\rho]$. But this approximation breaks down when the contributions to the entropy from the metastable state ρ_m becomes comparable to or less than the contributions from other states ρ' in a vicinity of ρ_m, $\|\rho_m - \rho'\| \ll \|\rho_m\|$. This happens when ρ_m ceases to be at least a local maximum of entropy, which is exactly what takes place at the metastability-instability transition points E_1 and E_2. This breakdown of the mean field approximation near the E_1 and E_2 energies can also be viewed as fluctuation-induced uncertainty in the exact location of the metastability-instability transition. It is shown in Ref. [20] that the relative uncertainty $\Delta E/E_1$ in the position of the collapse point E_1 scales with the number of particles as $N^{-2/3}$. Hence, given that N is large, the mean-field results are asymptotically exact for all energies except for those near the ends of metastable branches E_1 and E_2.

Another distinct feature of gravitational phase transitions is the anomalous stability of the metastable branches $[E_1, E^*]$ and $[E^*, E_2]$ (Fig. 1). Consider, for example, a metastable uniform state and a stable core-halo state both having the same energy somewhere in the middle of the interval $[E_1, E^*]$. The entropy minimum, that separates the entropy maxima corresponding to the stable and metastable states, has the depth ΔS which is proportional to the number of particles, i.e. $\Delta S = N\Delta s$ (for example, in Fig. 3 where Δs is equal to the difference in coordinates between the metastable (solid line) and unstable (dashed line) states, $\Delta s \approx 0.1$). Physically, this is so because the transition from a metastable uniform state to a stable core-halo state requires a macroscopic fluctuation equivalent to the rearrangement of the density distribution in the *whole* system. Hence, the probability of the metastable-stable transition is proportional to $\exp(-N\Delta s)$ and becomes prohibitively small even for a moderate number of particles N. Only near the ends of metastability branches E_1 and E_2 is the probability of metastability-stability transition significant; it is of order $\mathcal{O}(N^0)$ in the interval $[E_1, E_1 + \Delta E]$, where

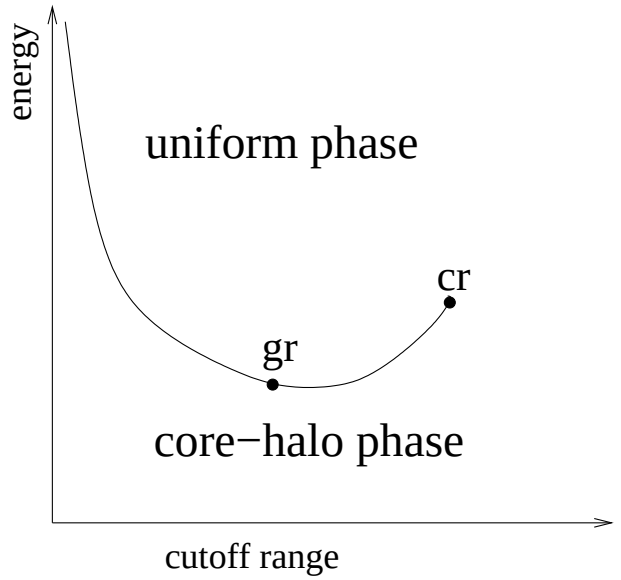

FIG. 11: Sketch of the phase diagram of a self-attracting system. The crossover point between the gravitational and first-order phase transition and the critical point are marked "gr" and "cr", respectively.

$\Delta E \sim E_1 N^{-2/3}$ [20].

Given the arguments presented above we conclude that the mean-field approximation adequately represents the phenomenology of self-attracting systems and correctly describes the gravitational, first-order, and second-order phase transitions.

V. CONCLUSION

In Sect. II and III we considered two examples of self-attracting systems, the ensemble of self-gravitating fermions and the ensemble of classical particles interacting via attractive soft Coulomb potential. These systems have a similar $\sim 1/r$ interaction at large distances but very different forms of short-range cutoffs. While in the second example the short-range cutoff is evidently r_0, in the first example the role of the short-range cutoff is indirectly played by the Pauli exclusion principle, which depends on the particle density. Despite this different small-r behavior, both of the considered ensembles exhibit the same sequence of phase transitions: gravitational, first-order, second-order, and none, as the range of their respective cutoffs is increased. The sketch of their phase diagram in cutoff-energy coordinates is represented in Fig. 11 and completes the one given in Ref. [10] in cutoff-temperature coordinates. The examples considered in this paper were chosen mainly because of the physical importance of the $1/r$ potential but similar phase diagrams exist for all nonintegrable $1/r^\alpha$, $0 < \alpha < 3$ attractive potentials. The main physical reason behind this phase diagram is that the short-range cutoff controls the maximum density a self-attracting system can achieve. As the range of the cutoff is increased, the collapsed central core becomes less dense and occupies more volume, and at some point the system has simply nowhere to collapse. It happens when the central density of the non-collapsed uniform state becomes similar to the core density of the collapsed core-halo state. Likewise, the critical point is reached when the maximum allowed density becomes so small that the system remains virtually uniform for any energy. The purely geometrical nature of these arguments indicates that the phase diagram, obtained in the previous two sections, should be robust and insensitive to such simplifying assumptions as spherical symmetry. The validity of the main approximation used in this paper, the mean-field approach, was discussed in Sec. IV. It is revealed that the mean-field approximation correctly describes the behavior of the self-attracting systems for all accessible energies and cutoff radii, excluding the immediate vicinities of the collapse points. We leave the study of the collapse points in the finite-particle systems as well as the dynamics of the collapse for a future paper.

VI. ACKNOWLEDGMENT

The authors are grateful to the organizers of the Les Houches Ecole de Physique meeting for providing an opportunity to discuss the results of this work. I. I. gratefully acknowledges the support of FONDECYT under grant 1020052.

[1] V. A. Antonov, Vest. Leningr. Gos. Univ. **7**, 135 (1962).
[2] D. Lynden-Bell and R. Wood, Mon. Not. R. Astr. Soc. **138**, 495 (1968).
[3] M. K.-H. Kiessling, J. Stat. Phys. **55**, 203 (1989).
[4] T. Padmanabhan, Phys. Rep. **188**, 285 (1990).
[5] B. Stahl, M. K.-H. Kiessling, and K. Schindler, Planet. Space Sci. **43**, 271 (1995).
[6] P.-H. Chavanis and J. Sommeria, Mon. Not. R. Astr. Soc. **296**, 569 (1998).
[7] V. P. Youngkins and B. N. Miller, Phys. Rev. E. **62**, 4583 (2000).
[8] I. Ispolatov and E. G. D. Cohen, Phys. Rev. E. **64**, 056103 (2001).
[9] H. J. de Vega and N. Sánchez, Nucl. Phys. B **625**, 409 (2002)
[10] P.H. Chavanis, Phys. Rev. E, in press [cond-mat/0109294].
[11] P.H. Chavanis, C. Rosier, and C. Sire, Phys. Rev. E, submitted [cond-mat/0107345].
[12] P.H. Chavanis, Astron. Astrophys. **381**, 340 (2002).
[13] D. H. E. Gross, *Microcanonical Thermodynamics: Phase Transitions in "Small" Systems*, Lecture Notes in

Physics, Vol. 66 (World Scientific, Singapore, 2001).
[14] I. Ispolatov and E. G. D. Cohen, Physica A **295**, 475 (2001).
[15] R. W. Gerling and A. Hüller, Z. Phys. B **90**, 207 (1993).
[16] S. Chandrasekhar, *An Introduction to the Study of Stellar Structure* (Dover Publications, 1958), Ch. 11.
[17] J. Binney and S. Tremaine *Galactic Dynamics* (Princeton Series in Astrophysics, 1987).
[18] J. Katz, Mon. Not. R. Astr. Soc. **183**, 765 (1978).
[19] G. Horwitz and J. Katz, Astrophys. J. **222**, 941 (1978).
[20] J. Katz and I. Okamoto, Mon. Not. R. Astr. Soc. **371**, 163 (2000).